Periodic traveling waves in a taut cable on a bilinear elastic substrate

Lucio Demeio

Dipartimento di Scienze Matematiche
Università Politecnica delle Marche
Via Brecce Bianche 1
I-60131 Ancona, Italy
(corresponding author)
e-mail: demeio@mta01.univpm.it
and

Stefano Lenci

Dipartimento di Architettura, Costruzioni e Strutture
Università Politecnica delle Marche
Via Brecce Bianche 1
I-60131 Ancona, Italy
e-mail: lenci@univpm.it

Abstract

The wave propagation problem on a taut cable resting on a bilinear substrate is investigated, without and with a distribute transversal load. The piecewise nature of the problem offers a sufficiently simple kind of nonlinearity as to permit a closed form solution both for the wave phase velocity and the wave form. We show that the solution depends only on the ratio between the two soil stiffnesses, and that no waves propagate if one side of the substrate is rigid. Some numerical simulations, based on a finite difference method, are performed to confirm the analytical findings. The stability of the proposed waves is discussed analytically and numerically.

1 Introduction

Within the realm of nonlinear problems in science and engineering, an important role is played by the piecewise linear systems [1–4]. In fact, from the one side, they have all the characteristics, and complexity, of nonlinear models, with a cornucopia of cases and phenomena to be avoided or exploited, many more than in the linear case. From the other side, they often possess closed form solutions, which are useful for the full understanding and for the possibility of performing detailed parametric analyses, seldom feasible by numerical means [5–7]. Also, sometimes the piecewise linear system has a richer dynamics than the smooth nonlinear counterpart [8, 9].

Among the many examples of piecewise linear systems in engineering applications, we mention the inverted pendulum with lateral barriers [10,11], oscillations of rigid blocks [12], vibro-impact systems [13,14], cracked beams [15–17] (where the crack is treated as a bilinear lumped spring), capsule systems [18], drillstring problems [19] and neuronal networks with gap junctions [20]. Referring to continuous systems, relevant examples are those of beams and cables resting on unilateral foundations [21–24].

In this paper we consider the wave propagation in a taut cable, or string, resting on a piecewise linear foundation, which is a paradigmatic example of a continuous bilinear system and contains a simple form of nonlinearity. In mathematical language the wave equation with the addition of a restoring term is known as the Klein-Gordon equation [25], and arises, among others, in quantum mechanics. When the restoring term is linear in the displacement we obtain the linear Klein-Gordon equation, while other shapes of the restoring term, including a piecewise linear expression, lead to a nonlinear Klein-Gordon equation. As is well known, the same equation holds for axial and torsional wave propagating in beams and in other physical systems.

Although wave propagation in taut cables is a well-known and well investigated problem [26, 27], even in the presence of an elastic foundation, to the best of our knowledge the problem with a piecewise linear distributed support has not been previously addressed, and we hope to fill this gap. In fact, while the dynamics of beams resting on bilinear foundations has been investigated by various authors [28–37], to the best of our knowledge a similar analysis has not been done for the string, in spite of the simpler equation involved. For example, the recent extended review by Younesian et al. [38] does not mention this type of foundation, although it considers other nonlinear substrate models and although it affirms that "a foundation model may

present different behavior under tension and pressure loads". As a matter of fact, this work extends to strings the same problem studied in [37] for the beam.

A particular case is obtained when one of the two stiffnesses is zero, which corresponds to a unilateral substrate. This situation has been considered in [39] for the case of two moving lumped forces, although the problem of free wave propagation is not addressed directly. This problem finds application, for example, in railway overhead power lines. Actually, this engineering example constitutes one of the practical problems which triggered this study. The case of a cable in between two different media (for example in underground power lines) or that of filaments resting on two different tissues (in biomechanics) and other interface problems are further examples. Referring to the engineering case of axial wave propagation in beams, it finds applications in foundation piles, since in general the surrounding soil does not have a symmetrical behaviour.

The findings of this paper can be potentially used in the field of architectured materials, or metamaterials, where the material is properly designed and tailored to obtain specific wave propagation properties, related to the loss of symmetrical behaviour [40]. Another element of novelty of the present work is that the stability problem is addressed. Again, the stability has been investigated for beams in [37] with a technique similar to the one herein employed, and in [41], although in this latter work the bilinear substrated has been approximated by a smoother function, but not for strings. This problem is challenging, and will be addressed analytically only for a subset of possible perturbations around the considered propagating waves, and numerically for more generic perturbations.

We consider traveling waves of wavelength L and whose shape changes sign at least once within the wavelength. If there is only one change of sign within the wave length L we name it "single wave" (Fig. 1a); this is the solution of main interest in this work. If the change of sign occurs in more than one point within the wavelength we name it "multiple wave" (Fig. 1b).

By repeating n times a single wave solution we (trivially) obtain a multiple wave solution of wave length nL, which we name "repetitive multiple wave". Although it represents the same physical wave, it is a different solutions of the mathematical problem which we will introduce in our analytical computations, because we will use the wavelength L to define a nondimensional space variable. Thus, repetitive multiple waves must be considered in com-
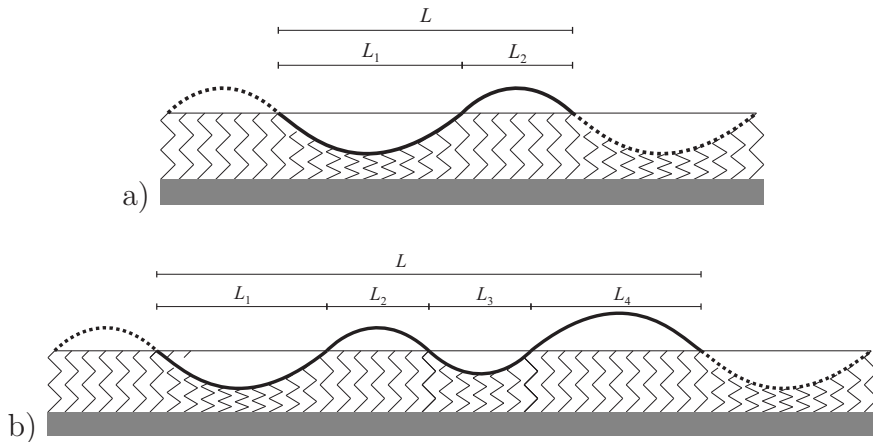
Figure 1: a) Single wave and b) multiple wave travelling periodic solutions.

putations, even if they do not represent new physical solutions and the only interesting case is with $n = 1$.

The paper is organized as follows: in Section 2 we introduce the problem, the equations and the periodic-wave analytical solutions; in Section 3 we present some numerical simulations and Section 4 contains our conclusions.

2 Governing equations and analytical solutions

The governing equation for a taut cable on a general nonlinear substrate and without external excitation is given by the nonlinear Klein-Gordon equation [42, 43]

$$\frac{\partial^2 w}{\partial t^2} - v^2 \frac{\partial^2 w}{\partial x^2} + \gamma(w)\, w = 0, \tag{1}$$

where $w(x,t)$ is the cable profile with respect to the substrate, $x \in \mathbb{R}$ is the space variable, $t \geq 0$ the time, $v = \sqrt{T/\rho}$ is the wave phase speed in absence of the substrate (ρ is the mass per unit length and T the tension of the cable), and $\gamma(w)$ is the stiffness of the substrate. For different mechanical problems, governed by the same equation, the wave speed v has different expressions.

We shall investigate the existence and the functional form of traveling wave solutions of equation (1) for the case of a bilinear substrate, i.e. for a piece-wise constant stiffness function $\gamma(w)$. For the purpose of the numerical simu-

4

lations, we shall also consider the associated initial/boundary value problem

$$\frac{\partial^2 w}{\partial t^2} - v^2 \frac{\partial^2 w}{\partial x^2} + \gamma(w)\, w = 0, \quad x \geq 0, \tag{2}$$

$$w(0, t) = \varphi(t), \tag{3}$$

$$w(x, 0) = w_0(x), \qquad \frac{\partial w}{\partial t}(x, 0) = \psi(x), \tag{4}$$

where $\varphi(t)$, $w_0(x)$ and $\psi(x)$ are given functions. When the initial value problem given by equations (2) and (4) is posed over the whole real line, the total energy is conserved if the initial condition $(w_0(x), \psi(x))$ has compact support. If the problem is considered on the half-space $x \in \mathbb{R}^+$ with the boundary condition imposed in (3) the total energy is not conserved, but it is easy to recover an expression for its time dependence. Let

$$T(t) = \int_0^\infty \frac{1}{2} \left(\frac{\partial w}{\partial t}\right)^2 dx, \tag{5}$$

$$V(t) = \int_0^\infty \left\{ \frac{1}{2} \left(v \frac{\partial w}{\partial x}\right)^2 + \Gamma(w) \right\} dx, \tag{6}$$

$$E(t) = T(t) + V(t), \tag{7}$$

where $\Gamma(w)$ is a primitive of $\gamma(w)\, w$, be the kinetic energy, the potential energy and the total energy for the half-space problem. We then have:

$$\frac{dE}{dt} = \frac{d}{dt} \int_0^\infty \left\{ \frac{1}{2} \left(\frac{\partial w}{\partial t}\right)^2 + \frac{1}{2} \left(v \frac{\partial w}{\partial x}\right)^2 + \Gamma(w) \right\} dx =$$

$$= \int_0^\infty \left\{ \dot{w}\, \ddot{w} + v^2\, w'\, \dot{w}' + \gamma(w)\, w\, \dot{w} \right\} dx =$$

$$= \lim_{R \to \infty} \int_0^R \left\{ \dot{w}\, \ddot{w} + v^2\, w'\, \dot{w}' + \gamma(w)\, w\, \dot{w} \right\} dx. \tag{8}$$

After integrating the second term by parts and assuming that the initial condition has compact support we have:

$$\frac{dE}{dt} = \lim_{R \to \infty} \left\{ \int_0^R \left(\dot{w}\, \ddot{w} - v^2\, w''\, \dot{w} + \gamma(w)\, w\, \dot{w} \right) dx + v^2 \left[w'\, \dot{w} \right]_0^R \right\} =$$

$$= \lim_{R \to \infty} \left\{ \int_0^R \dot{w} \left(\ddot{w} - v^2\, w'' + \gamma(w)\, w \right) dx + v^2 \left[w'\, \dot{w} \right]_0^R \right\} =$$

$$= -v^2 \frac{\partial w}{\partial x}(0, t) \frac{\partial w}{\partial t}(0, t) = -v^2\, \dot{\varphi}(t) \frac{\partial w}{\partial x}(0, t), \tag{9}$$

where it has been taken into account that $\ddot{w} - v^2\,w'' + \gamma(w)\,w = 0$ because of (2) and that

$$\lim_{R \to \infty} \frac{\partial w}{\partial x}(R,t)\,\frac{\partial w}{\partial t}(R,t) = 0$$

because of the compactness of the support of the initial condition. We have used equation (9) as a benchmark in some of our numerical simulations.

2.1 Periodic solutions

We look for traveling wave periodic solutions of equation (1), that is continuously differentiable solutions of the form

$$w(x,t) = W(s), \tag{10}$$

with $s = x - \hat{c}\,t$; for convenience, we introduce the nondimensional variables

$$c = \frac{\hat{c}}{v}, \quad k(W) = \gamma(W)\,\frac{L^2}{v^2}, \quad \xi = \frac{s}{L}, \tag{11}$$

where L is the wavelength. By substituting equations (10) and (11) in (1) we obtain the following ordinary differential equation for $W(\xi)$

$$(c^2 - 1)\,W''(\xi) + k(W)\,W(\xi) = 0, \tag{12}$$

whose solution for $\xi \in [0,1]$ provides the functional form of the traveling wave within one wavelength.

In this work, the substrate stiffness is represented by the piecewise constant function

$$k(W) = k_1, \quad W \le 0 \tag{13}$$
$$k(W) = k_2, \quad W > 0 \tag{14}$$

for real positive constants k_1 and k_2. Accordingly, let W_1 and W_2 be the restrictions of the profile function $W(\xi)$ to the intervals characterized by the sign of W, namely $W(\xi) = W_1(\xi)$ if $W \le 0$ (compression interval) and $W(\xi) = W_2(\xi)$ if $W > 0$ (tension interval). Note that, by the symmetry of the equations, if $W(\xi)$ is a solution corresponding to a propagation velocity c for given values of the stiffnesses k_1 and k_2, then $-W(\xi)$ is the solution with the same propagating speed c and the stiffnesses reversed ($k_1 \to k_2$, $k_2 \to k_1$). This allows us to consider only the case $k_1 \le k_2$.

6

With (13) and (14) equation (12) becomes a system of two differential equations for the two functions W_1 and W_2,

$$(c^2 - 1)\frac{d^2 W_1}{d\xi^2}(\xi) + k_1 W_1(\xi) = 0, \quad \text{for} \quad W_1(\xi) \leq 0, \tag{15}$$

$$(c^2 - 1)\frac{d^2 W_2}{d\xi^2}(\xi) + k_2 W_2(\xi) = 0, \quad \text{for} \quad W_2(\xi) > 0. \tag{16}$$

Equation (12) or the equivalent equations (15)-(16) form a nonlinear eigenvalue problem of the second type [44–46]. For any given value of k_1 and k_2 we expect a multiplicity of solutions, some (often only one) of which correspond to the single wave solutions under investigation, while others are expected to be multiple waves.

As anticipated in the introduction, we are interested in single wave solutions which change sign only once in the interval $(0, 1)$; with an appropriate choice of the reference frame, this is equivalent to say that there exists one $\alpha \in (0, 1)$ such that $W(0) = W(\alpha) = W(1) = 0$, $W(\xi) = W_1(\xi) < 0$ for $0 < \xi < \alpha$ and $W(\xi) = W_2(\xi) > 0$ for $\alpha < \xi < 1$. The dimensionless spatial extension of the two intervals are then α and $1 - \alpha$, their physical extensions (in the s variable) being $L_1 = \alpha L$ and $L_2 = (1 - \alpha) L$, respectively. The wavelength L is then a free scaling parameter, while L_1 and L_2 have to be determined as part of the solution. Thus, this is a free boundary problem.
With

$$a^2 = \frac{k_1}{c^2 - 1}, \quad b^2 = \frac{k_2}{c^2 - 1}, \tag{17}$$

the solution of (15)-(16) can be written in the form

$$W_1(\xi) = c_1 \sin(a\xi) + c_2 \cos(a\xi), \tag{18}$$
$$W_2(\xi) = c_3 \sin(b(\xi - \alpha)) + c_4 \cos(b(\xi - \alpha)), \tag{19}$$

which, together with (10), implies that only mono-harmonic waves can propagate. The solution of equations (15)-(16) is determined up to an arbitrary multiplicative constant; one of the four constants c_1, c_2, c_3, c_4 will therefore remain undetermined. Note that $b = a\sqrt{k_2/k_1}$, and that a and b must be real otherwise the solution would be hyperbolic and it would not be possible to fulfill the boundary conditions with a non-trivial solution. This entails $c > 1$, i.e. the physical phase velocity $\hat{c}$ must be greater than v, as expected since with the soil the system is stiffer and the velocity of wave propagation is larger.

The boundary conditions on W_1 and W_2 at $\xi = 0$, $\xi = \alpha$ and $\xi = 1$ are given by the continuity of the function W and of its slope. Continuity and periodicity of the function gives

$$W_1(0) = 0, \tag{20}$$
$$W_1(\alpha) = 0, \tag{21}$$
$$W_2(\alpha) = 0, \tag{22}$$
$$W_2(1) = 0, \tag{23}$$

which entail $c_2 = c_4 = 0$, and

$$a\,\alpha = \pi \quad \text{and} \quad b(1-\alpha) = \pi. \tag{24}$$

By substituting equations (24) into (17) we obtain the following relationships between the phase velocity c and the parameter α:

$$c^2 = 1 + \frac{k_1\alpha^2}{\pi^2}, \tag{25}$$

$$c^2 = 1 + \frac{k_2\,(1-\alpha)^2}{\pi^2}, \tag{26}$$

from which we can determine α and c in terms of k_1 and k_2 for single traveling waves:

$$\alpha = \frac{\sqrt{k_2}}{\sqrt{k_1} + \sqrt{k_2}} = \frac{1}{1 + \sqrt{k_1/k_2}} \tag{27}$$

$$c^2 = 1 + \frac{1}{\pi^2}\frac{k_1\,k_2}{(\sqrt{k_1} + \sqrt{k_2})^2}. \tag{28}$$

We see that α (and therefore the shape of the solution) is a function only of the ratio k_1/k_2 and not of k_1 and k_2 separately.

For the sake of completeness, we also report the boundary conditions in the case of a repetitive multiple wave solution; only equation (23) would change into

$$W_2\left(\frac{1}{n}\right) = 0 \tag{29}$$

which implies

$$\alpha = \frac{1}{n}\frac{\sqrt{k_2}}{\sqrt{k_1} + \sqrt{k_2}} = \frac{1}{n}\frac{1}{1 + \sqrt{k_1/k_2}}, \tag{30}$$

$$c^2 = 1 + \frac{1}{(n\,\pi)^2}\frac{k_1\,k_2}{(\sqrt{k_1} + \sqrt{k_2})^2}. \tag{31}$$

Note that in principle other multiple wave solutions, *non repetitive*, are possible. Expressions (30) and (31) show that the eigenvalues form a countably infinite set.

Returning to the single wave case, the boundary conditions on the continuity of the slopes are given by

$$W_1'(0) = W_2'(1),\tag{32}$$
$$W_1'(\alpha) = W_2'(\alpha),\tag{33}$$

which entail $c_1 = -c_3\sqrt{k_2/k_1}$ and equation (33) is automatically satisfied (this can be easily understood from geometrical considerations, since the slope of the sine function at π is opposite to the slope at 0).

By collecting all results, the solution of equations (15)-(16) becomes:

$$W_1(\xi) = -c_3\sqrt{\frac{k_2}{k_1}}\sin\left(\frac{\xi\pi}{\alpha}\right), \quad 0 \le \xi \le \alpha,\tag{34}$$

$$W_2(\xi) = c_3\sin\left(\frac{(\xi-\alpha)\pi}{1-\alpha}\right), \quad \alpha \le \xi \le 1,\tag{35}$$

where α is given by (27), and c_3 is the undetermined amplitude of the wave which can be chosen by some normalization. The period and the frequency of the wave are given by

$$\tau = \frac{L}{c\,v}, \qquad \omega = \frac{2\,\pi}{\tau}.\tag{36}$$

2.2   Stability

The stability of periodic solutions with a bilinear stiffness term has been studied only with regard to specific situations or with drastic model assumptions which essentially change the nature of the problem in the context of the beam equation [41]. In [42] the stability of the solutions for the Klein-Gordon equation has been addressed in a quantum-mechanical context with a regular stiffness term. Here, we provide some basic results on the issue, by using some general theoretical considerations (see here below) and by numerical means (see section 3), without the pretense of giving an exhaustive and complete view.

It is easy to see that the periodic solutions of equations (15)-(16) are *orbitally stable (but not stable in the Lyapunov sense nor asymptotically stable) with*

9

respect to perturbations of the form given by (10). First of all, we note that the phase portrait $(W(\xi), W'(\xi))$ $0 \leq \xi \leq 1$, of the solutions of (15)-(16) is made of two half ellipses, of different vertical semi-axis and connected at $W_1 = W_2 = 0$. The previous statement can be made more precise, still remaining within the perturbations given by (10), by regarding the system (15)-(16) as a map from $\xi = 0$ to $\xi = 1$; our periodic solution is then a fixed point of this map at $(W(0), W'(0)) = (0, -c_3\sqrt{\frac{k_2}{k_1}}\frac{\pi}{\alpha})$. The linearization of the map near the fixed point can easily be constructed by considering a small perturbation to the initial condition at $\xi = 0$. The Jacobian of the map at the periodic orbit can then be calculated and it easy to see that the two Floquet multipliers are both equal to $+1$. This proves the orbital stability with respect to the perturbations of the form given by (10).

More detailed investigations on the stability of the periodic solutions of equation (15)-(16) will be carried out by numerical means in section 3, both with respect to perturbations on the boundary conditions (3) and on the initial conditions (4).

2.3 Particular cases

When $k_1 = k_2 = k$ the substrate is linear and the solution is well known [26, 27]. We have

$$\alpha = \frac{1}{2}, \quad c^2 = 1 + \frac{k}{(2\pi)^2}, \tag{37}$$

and $W(\xi)$ is a simple sine function.

2.3.1 Unilateral substrate

When $k_2 \to 0$, the substrate becomes unilateral. In this limit we have $\alpha \to 0$, $c \to 1$ and $W_1(\xi) \to 0$ (see (27), (28), (34) and (35)), which means that the wave propagates with the same speed as in the absence of the substrate and the compression region reduces to one point $(s = 0)$. An example of the solution over a two-period interval is reported in Fig. 2a, from which it is possible to see that the solution remains in the tension part. In addition, the derivative has a jump (Fig. 2b), since

$$\lim_{k_2 \to 0} W_1'(\xi) \approx \lim_{k_2 \to 0} \cos\left(\frac{\pi\xi n\sqrt{k_1}}{\sqrt{k_2}}\right) \tag{38}$$

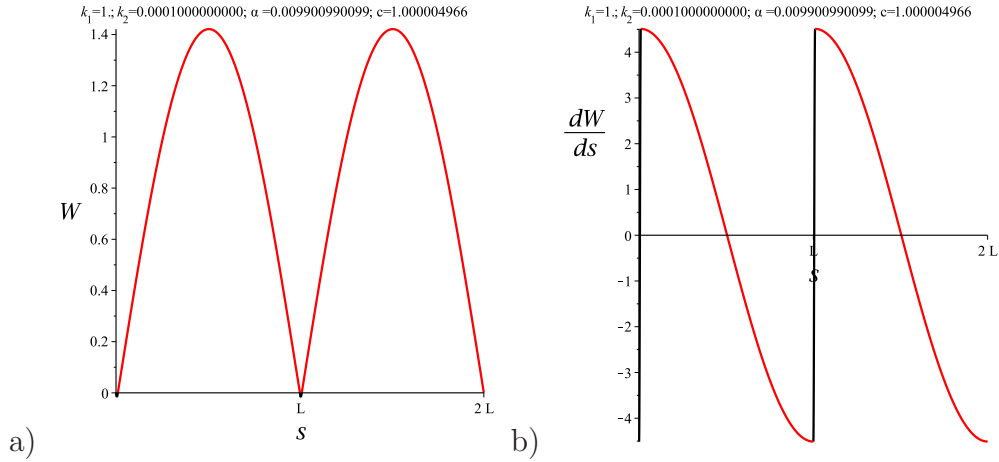is undefined, although bounded in a neighborhood of $k_2 = 0$.

10

Figure 2: The solution $W(s)$ for $k_1 = 1$ and $k_2 = 10^{-4}$. $n = 1$.

The conclusion is that periodic waves with regular profile on a perfectly unilateral substrate, crossing the region $w < 0$ (where $k_1 > 0$) do not exist. Of course, in this case waves of arbitrary shape (because of the D'Alembert solution) can propagate remaining always in the detached part $w > 0$.

This result can be interpreted also from a mechanical point of view. In fact, in the region $w > 0$ ($k_2 = 0$) the wave propagates with velocity $c = 1$ (see (26)), while in the region $w < 0$ ($k_1 > 0$) it would propagate with velocity $c > 1$ (see (25)), and thus it is not possible to match them.

2.3.2 Unilaterally rigid substrate

When $k_2 \to \infty$, one side of the substrate becomes rigid. In this limit $\alpha \to 1$, $c \to 1 + k_1/\pi^2$ and $W_2(\xi) \to 0$ (see (27), (28), (34) and (35)), which means that the detached tension region reduces to one point ($s = L$) and a non-vanishing solution exists only on the side of the deformable substrate. An example is reported in Fig. 3a. Also in this case the derivative has a jump (Fig. 3b) since

$$\lim_{k_2 \to \infty} W_2'(\xi) \approx \lim_{k_2 \to \infty} \cos\left(\frac{\pi \xi n \sqrt{k_2}}{\sqrt{k_1}}\right) \tag{39}$$

is undefined, although bounded as $k_2 \to \infty$.

The conclusion is that periodic waves with regular profile on unilaterally rigid substrate do not propagate in taut cables.
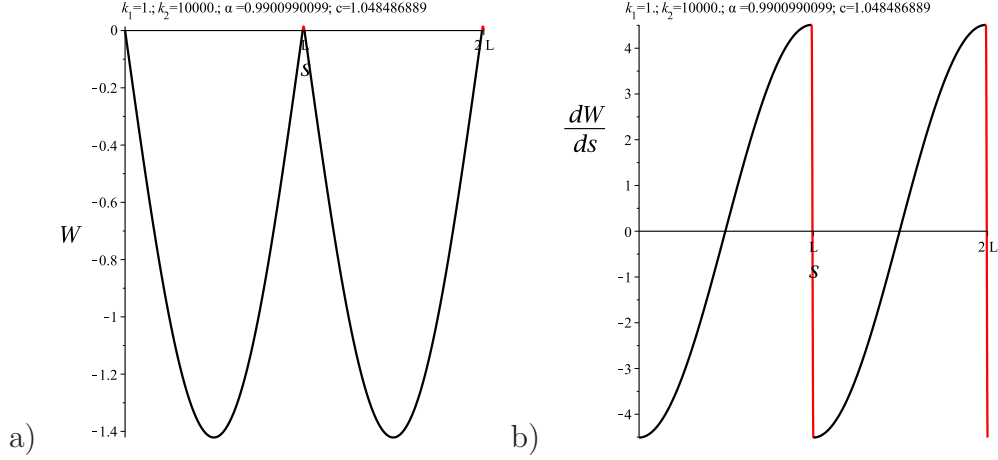
11

Figure 3: The solution $W(s)$ for $k_1 = 1$ and $k_2 = 10^4$. $n = 1$.

In this case, as it results from equations (18)-(19) and at variance with the situation of section 2.3.2, no totally confined solution exists in the in-contact compression interval ($w < 0$ with strict inequality) at all.

2.3.3 Transverse distributed load

When a fixed, constant transverse distributed load $\hat{p} = \tilde{p}/\rho \in \mathbb{R}$ is present equation (1) becomes

$$\frac{\partial^2 w}{\partial t^2} - v^2 \frac{\partial^2 w}{\partial x^2} + \gamma(w)\, w = \hat{p}. \tag{40}$$

Also in this case, we look for solutions of the form (10) with the substrate stiffness given by equations (13)-(14). By using the dimensionless variables introduced in (11), the equations for W_1 and W_2 (analogous to equations (15) and (16)) are

$$(c^2 - 1)\frac{d^2 W_1}{d\xi^2}(\xi) + k_1 W_1(\xi) = p, \quad \text{for} \quad W_1(\xi) \leq 0, \tag{41}$$

$$(c^2 - 1)\frac{d^2 W_2}{d\xi^2}(\xi) + k_2 W_2(\xi) = p, \quad \text{for} \quad W_2(\xi) \geq 0, \tag{42}$$

where $p = \hat{p}\, \rho\, L^2/T = \hat{p}L^2/v^2 = \tilde{p}L^2/T$ and the solution is given by

$$W_1(\xi) = c_1 \sin(a\xi) + c_2 \cos(a\xi) + \frac{p}{k_1}, \tag{43}$$

$$W_2(\xi) = c_3 \sin(b(\xi - \alpha)) + c_4 \cos(b(\xi - \alpha)) + \frac{p}{k_2}. \tag{44}$$

12

Note that equations (43)-(44) support traveling wave solutions with arbitrary phase velocity and which do not change sign on the periodicity interval. This occurs when $\sqrt{c_1^2 + c_2^2} < |p/k_1|$ with $p < 0$ or $\sqrt{c_3^2 + c_4^2} < |p/k_2|$ with $p > 0$, i.e. if the oscillating part is smaller that the constant one. The solution in this case remains positive or negative, according to the sign of p, on the whole interval. The coefficients a and b (respectively) remain undetermined; according to the nomenclature introduced in Section 2.1 we call them "zero" wave solutions (because there are no points at which the solution vanishes).

The symmetry property of the periodic travelling solutions without the transverse external load, discussed in Section 2.1 immediately after equation (14), here involves the external load p as well: if $W(\xi)$ is a solution corresponding to a propagation velocity c for given values of the stiffnesses k_1 and k_2 and the external load p, then $-W(\xi)$ is the solution with the same propagating speed c and the stiffnesses reversed ($k_1 \to k_2$, $k_2 \to k_1$) and with $p \to -p$.

By imposing the boundary conditions (20)-(23) on the displacements we obtain the solutions which change sign on the periodicity interval; we have for the constants c_1, c_2, c_3 and c_4:

$$c_1 = \frac{p}{k_1}\frac{\cos(a\alpha) - 1}{\sin(a\alpha)}, \quad c_2 = -\frac{p}{k_1},$$
$$c_3 = \frac{p}{k_2}\frac{\cos[b(1-\alpha)] - 1}{\sin[b(1-\alpha)]}, \quad c_4 = -\frac{p}{k_2}. \tag{45}$$

It is easy to see, with some algebra, that

$$c_1^2 + c_2^2 = \left(\frac{p}{k_1}\right)^2 \sec^2\left(\frac{a\,\alpha}{2}\right) \geq \left(\frac{p}{k_1}\right)^2$$
$$c_3^2 + c_4^2 = \left(\frac{p}{k_2}\right)^2 \sec^2\left(\frac{b(\alpha-1)}{2}\right) \geq \left(\frac{p}{k_2}\right)^2$$

in agreement with the request that the solutions change sign over the period. Note also that they exist if and only if $a\alpha \neq \pi$ and $b(1-\alpha) \neq \pi$, which are complementary to the existence conditions (24) of the case without transverse load, which then comes out to be a special "resonant" case. An additional condition is given by the request that $W_1(\xi) \leq 0$ for $0 \leq \xi \leq \alpha$ and $W_2(\xi) \geq 0$ for $\alpha \leq \xi \leq 1$, for which it is sufficient that $W_1'(0) \leq 0$. By using equations (43) and (45) we obtain $W_1'(0) = a\,c_1 \leq 0$ which entails $c_1 \leq 0$, that is

$$\frac{p}{k_1}\frac{\cos(a\alpha) - 1}{\sin(a\alpha)} \leq 0. \tag{46}$$

13

This condition indicates that for $a\alpha \leq \pi$ we must have $p > 0$, while for $a\alpha \geq \pi$ we must have $p < 0$.

The two boundary conditions (32) and (33) on the derivatives are again linearly dependent (for the same geometrical reasons), and give, after some algebra,

$$\sqrt{\frac{k_1}{k_2}} = \frac{\sin(a\alpha)}{\cos(a\alpha) + 1} \frac{\sin\left[a\sqrt{\frac{k_2}{k_1}}(1-\alpha)\right]}{\cos\left[a\sqrt{\frac{k_2}{k_1}}(1-\alpha)\right] - 1}, \tag{47}$$

which provides a relationship between a and α in terms of the ratio k_1/k_2, e.g., $a = a(\alpha, k_1/k_2)$. With respect to the case without load, where for given values of k_1 and k_2 the parameters α and c are uniquely determined, here, instead, α can be chosen freely and a is then determined as the solution of the trascendental equation (47). Thus, we have a 1-parameter manifold of solutions. The value of α for which $a\,\alpha = \pi$, which is obtained when α, c and a are given by equations (17), (27) and (28), i.e. their expressions in the case without load, is crucial for the fulfillment of condition (46) and we shall call it α_{cr} (critical value): for $\alpha = \alpha_{cr}$ the solution of equations (43)-(47) ceases to exist and the amplitude of the wave, which is no longer a free parameter as in the absence of the load, but it depends on α, diverges in the limit; for $\alpha \leq \alpha_{cr}$ the solution exists for $p > 0$, while for $\alpha \geq \alpha_{cr}$ the solution exists for $p < 0$. We shall illustrate this fact by numerical examples in Section 3.

For a given α, a is determined by equation (47) and the propagation speed of the wave is then given by

$$c = \sqrt{1 + \frac{k_1}{a^2}}. \tag{48}$$

The solutions of equation (47) are reported in Fig. 4 as curves in the cartesian plane (α, a). The solid lines represent the solutions for $k_1 = 30$ and $k_2 = 1$ (red line), $k_1 = 3$ and $k_2 = 1$ (black line) and $k_1 = 0.1$ and $k_2 = 1$ (blue line). The dashed green line represents the first of the existence conditions (24), $a\,\alpha = \pi$ of the solution without load, while the other dashed lines represent the second of (24), $b\,(1-\alpha) = \pi$. The intersections of the dashed curves with the solid lines represent graphically the values of α_{cr} for the corresponding values of k_1 and k_2. Note that $a(0, k_1/k_2) = 2\pi\sqrt{k_1/k_2}$ and $a(1, k_1/k_2) = 2\pi$.
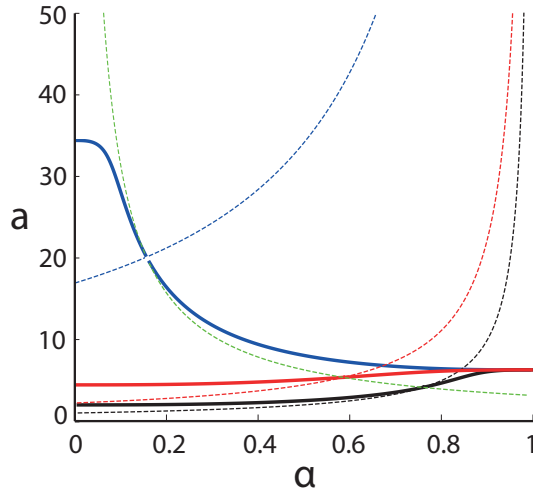
14

Figure 4: The solutions of equation (47) for $k_1 = 30, k_2 = 1$ (solid red line), $k_1 = 1, k_2 = 2$ (solid black line) and $k_1 = 1, k_2 = 10$ (solid blue line). The green dashed line represents the curve $a = \pi/\alpha$ corresponding to the case without load. The other dashed lines represent the second of (24), $b(1 - \alpha) = \pi$.

3   Numerical Simulations

This section is devoted to complement the analytic solutions found in Section 2 with some numerical investigations. A numerical solution of the wave equation (or, for that matter, of any evolution equation) can only be sought for in the form of a Cauchy problem, with a given set of initial and boundary conditions. Therefore, an exact reproduction of our periodic analytic solutions is not attainable; however, with a suitable choice of the initial and boundary conditions we can generate solutions which, after a relatively short transient, follow the pattern predicted by our analytic model in an interval of the whole real domain. The Cauchy problem for our simulations is given by equations (2)-(4) with the boundary condition $\varphi(t)$ equal to the analytical solution at $x = 0$,

$$\varphi(t) = w(0, t),$$

where $w(x, t)$ is the periodic solution given by (10), (34), (35) and the initial condition is $w_0(x) = \psi(x) = 0$. In addition, we impose that the numerical solution $w(x, t)$ vanishes at the end of the simulation domain. The undetermined amplitude (see equations (18), (19), (34) and (35) with the following discussions) is indicated by a_0 in the figure captions. With this choice, because of well-known properties of the wave equation [47], two symmet-

15

ric waves are generated at the origin, a left-propagating wave and a right-propagating wave. The latter, after an initial transient, becomes closer and closer to the periodic wave obtained analytically in Section 2, restricted to the half-space $x \geq 0$. We will use this scheme as verification of the properties of our analytic solutions and also as a mean to assess the stability of our waves, both with and without external distributed load. The algorithm is a simple finite-difference forward scheme, with the care of choosing the spatial discretisation and the time step properly in order to avoid numerical instabilities. Equation (9) has been used as a benchmark in all applicable cases and it is fulfilled with an accuracy of 10^{-4} to 10^{-5}.

3.1 No transverse distributed load
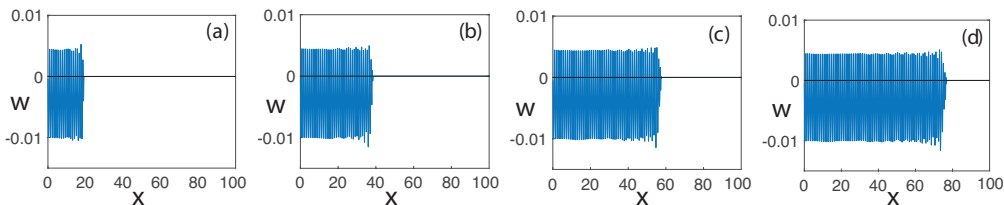
Figure 5: The solution $w(x,t)$ at four times for $k_1 = 1, k_2 = 5$ and $L = 1$, $a_0 = 0.01$: (a) $t = 20$, (b) $t = 40$, (c) $t = 60$, (d) $t = 80$.

The solution $w(x,t)$ without the external load is shown in Figures 5(a-d) and 6(a-d). Figures 5(a-d) show the progression of the periodic traveling wave with snapshots at constant time intervals for $L = 1$, $a_0 = 0.01$ and $k_1 = 1, k_2 = 5$; they illustrate how the wave generated by the boundary condition at the origin propagates into the initially empty half-space $x \geq 0$ with a phase speed consistent (within numerical errors) with the speed given by equation (28). An initial transient is formed on the head of the wave front and propagates to the right, while in an increasingly larger portion of the domain the solution settles to a right-propagating wave with constant amplitude, which is the restriction to $x \geq 0$ of the wave found analytically in Section 2 (the wave profile at the final time is shown in figure 6(b)). Figures 6(a-d) show the solution at the final time of our simulations for $L = 1$, $a_0 = 0.01$ and (a) $k_1 = k_2 = 1$, (b) $k_1 = 1, k_2 = 5$, (c) $k_1 = 0.2, k_2 = 1$, (d) $k_1 = 0.001, k_2 = 1$. The solution portrayed in Figure 6(a) corresponds to the bilateral case; the maximum excursions in Figures 6(b,c), both for $w > 0$ and $w < 0$ correspond to the excursions extracted analytically from equations (34) and (35). The solution shown in Figure 6(d), with a very
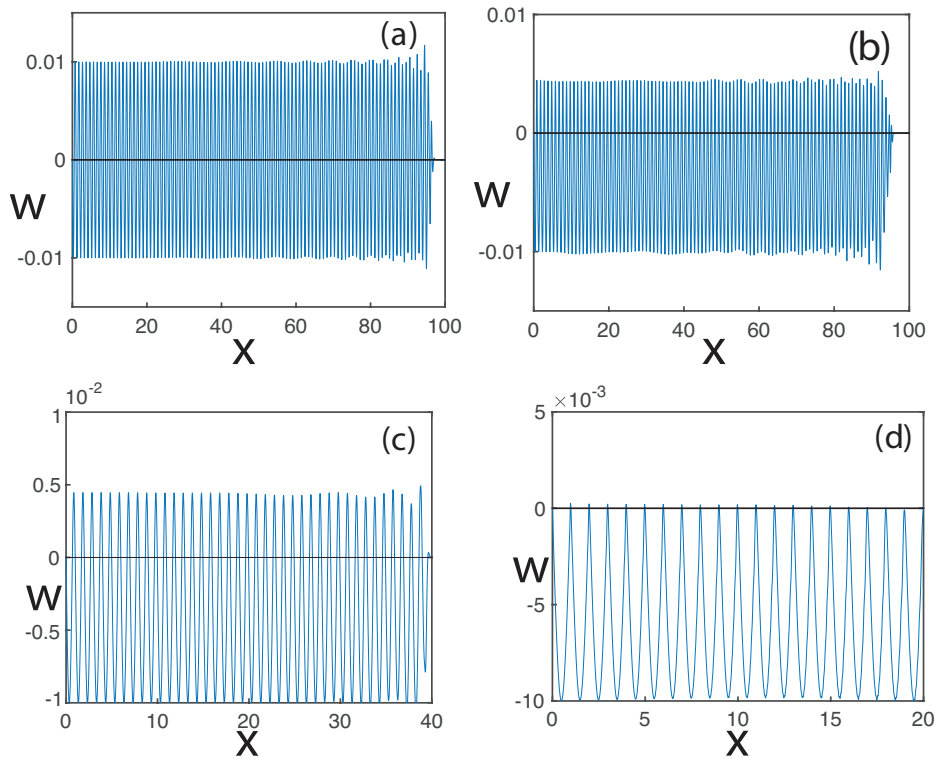
16

Figure 6: The solution $w(x,t)$ at the final time for (a) $k_1 = k_2 = 1$ (linear case), (b) $k_1 = 1, k_2 = 5$, (c) $k_1 = 0.2, k_2 = 1$, (d) $k_1 = 0.001, k_2 = 1$ and $L = 1$, $a_0 = 0.01$.

small value of k_1, corresponds to the limit of Subsection 2.3.2, with the proviso that, instead of $k_2 \to \infty$, we have chosen $k_1 \to 0$. We note that in this case, according to the theoretical results of section 2.3.1, non differentiable points appear at the endpoints of the spatial period. In all cases covered by our simulations (including the many ones not shown in this paper) only the initial transient depends upon the stiffnesses k_1 and k_2 separately, while the amplitude and the frequency of the final right-propagating wave depends only upon the ratio k_1/k_2, in agreement with the theoretical model. Finally, we remark that the choice of following the solution for a different number of periods in each case is due to numerical reasons, since the algorithm requires smaller time steps as $k_1 \to 0$ (or $k_2 \to \infty$), so we stop the simulation when the long-time behaviour is evident. The effect of the nonlinearity of the model when $k_1 \neq k_2$ is evident from the asymmetry of the wave profile with respect to the $w = 0$ baseline; the effect becomes more pronounced in the limiting cases of unilateral and unilaterally rigid substrate. The same

17

pattern observed in Figures 6(a-d) is also observed on a wide range of values in the (k_1, k_2) parameter space.

To address the stability properties of the periodic solutions obtained in the previous sections, we follow numerically solutions starting in the vicinity of the periodic traveling waves. We do so in two different ways: by imposing a small harmonic perturbation to the boundary condition or by choosing a small non-zero initial condition. With the first approach, let

$$\varphi(t) = w(0, t) + \varepsilon \sin(\omega_1 t). \tag{49}$$

be the boundary condition, with $\psi(x) = 0$. In Figure 7(a-c) we show the solution $w(x, t)$ for $k_1 = k_2 = 1$ (bilateral or linear case), with (a) $\varepsilon = 0.001$, (b) $\varepsilon = 0.003$, (c) $\varepsilon = 0.005$, $L = 1$, $a_0 = 0.01$ and $\omega_1 = 1.1\,\omega$, with ω defined in equation (36). The effect of the perturbation is to produce an oscillating amplitude at a frequency corresponding to $\omega_1 - \omega$. The amplitude of the slower oscillations is proportional to ε. The same behaviour is observed for $k_1 = 1, k_2 = 5$ in Figures 8(a-c) and for $k_1 = 0.001, k_2 = 1$ in Figures 9(a-c)
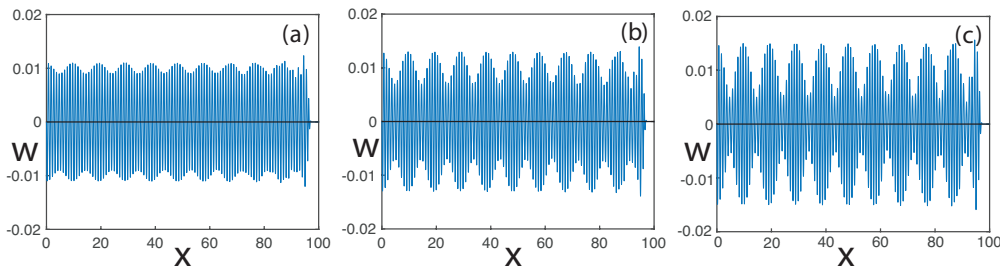

Figure 7: The solution $w(x, t)$ for $k_1 = k_2 = 1$ (linear case), with (a) $\varepsilon = 0.001$, (b) $\varepsilon = 0.003$, (c) $\varepsilon = 0.005$, $L = 1$, $a_0 = 0.01$ and $\omega_1 = 1.1\,\omega$.

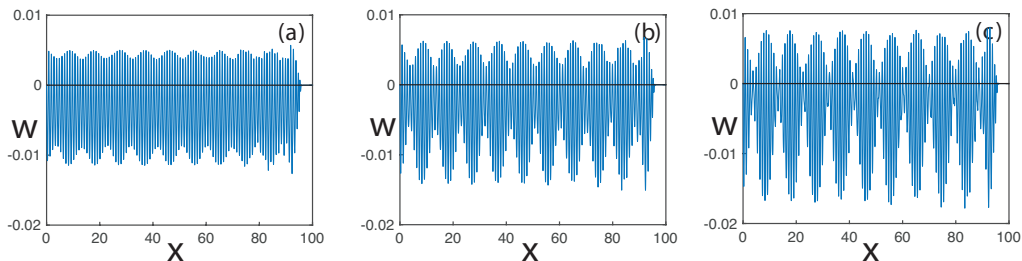

Figure 8: The solution $u(x, t)$ for $L = 1$, $a_0 = 0.01$, $k_1 = 1, k_2 = 5$, $\omega_1 = 1.1\,\omega$ and (a) $\varepsilon = 0.001$, (b) $\varepsilon = 0.003$, (c) $\varepsilon = 0.005$.
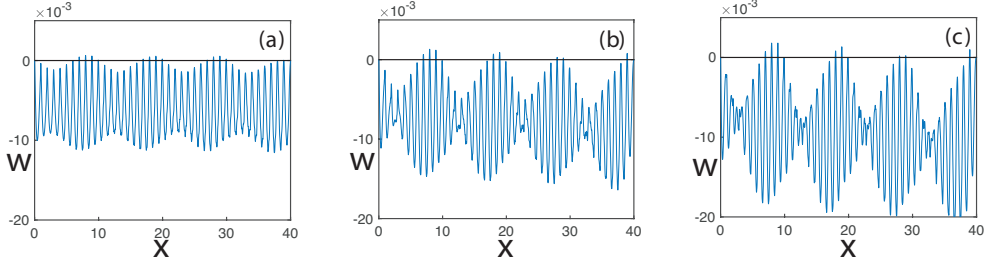
18

Figure 9: The solution $u(x,t)$ for $L = 1$, $a_0 = 0.01$, $k_1 = 0.001, k_2 = 1$, $\omega_1 = 1.1\,\omega$ and (a) $\varepsilon = 0.001$, (b) $\varepsilon = 0.003$, (c) $\varepsilon = 0.005$.

A convenient representation of the solutions is provided by the map $(f(t), \dot{f}(t)) \rightarrow (f(t+\tau), \dot{f}(t+\tau))$ of the phase space $(f(t), \dot{f}(t))$ onto itself, where $f(t) = w(x_0, t)$ with $x_0 > 0$ a suitably chosen point on the simulation domain and τ the period defined in equation (36). In rigorous terms, the map is independent of x_0. The return maps are shown in Figures 10(a-c) for (a) $k_1 = 1, k_2 = 1$, (b) $k_1 = 1, k_2 = 5$, (c) $k_1 = 0.001, k_2 = 1$.

The black dot at the center represents the unperturbed solution, the sets of blue, red and green dots around it correspond to $\varepsilon = 0.001$, $\varepsilon = 0.003$ and $\varepsilon = 0.005$, respectively. We see that the phase space points with $\varepsilon \neq 0$ lie on a closed orbit around the unperturbed fixed point, suggesting linear stability, as anticipated in Subsection 2.2. The different choice of $\omega_1 = \sqrt{2}\,\omega$ instead of $\omega_1 = 1.1\,\omega$ adopted in the previous simulations, is dictated by graphical reasons, since it gives a more densely populated phase-space trajectory. Note that the closed orbits around the unperturbed fixed point are of elliptical shape in the linear case ($k_1 = k_2$) while they appear more and more deformed as the difference between k_1 and k_2 becomes larger, thus making the nonlinearity more important.
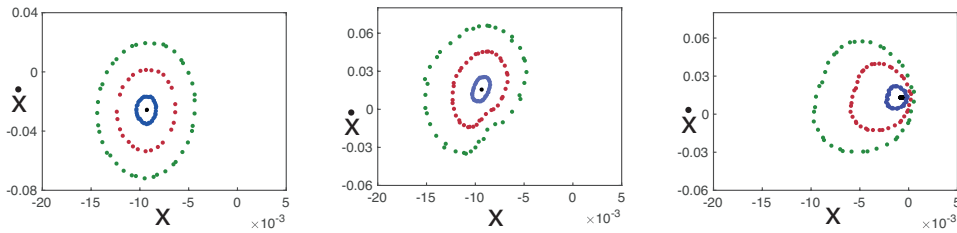

Figure 10: Return map for $L = 1$, $a_0 = 0.01$, $\omega_1 = \sqrt{2}\,\omega$, (a) $k_1 = k_2 = 1$ (linear case), (b) $k_1 = 1, k_2 = 5$, (c) $k_1 = 0.001, k_2 = 1$ and $\varepsilon = 0$ (black dot), 0.001 (blue dots), 0.003 (red dots) and 0.005 (green dots).

It is also to be noted that, as $k_1 \rightarrow 0$, the orbits surrounding the fixed point

tend to become tangent to each other, the periodic point becoming embedded in these curves at their point of contact. This is due to the fact that, as shown before, in this case the solution tends to stay only in the $w < 0$ region.

When perturbing the initial condition with a non-zero function, we must assure that the perturbed initial condition vanishes on a significant portion of the computational domain near its end, otherwise unwanted waves would propagate inwards from the right boundary.
For the example which we illustrate in figures 11(a,b) and 12(a,b) we have

$$w_0(x) = \varepsilon_1 \, \sin(\sqrt{2}\,x) \, \exp(-0.8\,x). \tag{50}$$

and (a) $k_1 = 1, k_2 = 2$, (b) $k_1 = 1, k_2 = 5$ and let ε_1 vary parametrically as we did before.
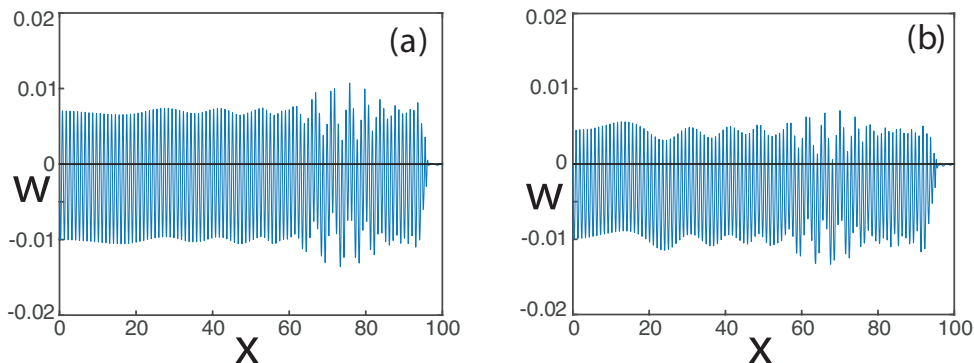

Figure 11: The solution $w(x, t)$ with the initial condition (50) for $L = 1$, $a_0 = 0.01$, (a) $k_1 = 1, k_2 = 2$, (b) $k_1 = 1, k_2 = 5$, and $\varepsilon = 0.0003$.

The behavior of the solution follows again the pattern of an initial transient with a subsequent settling to the travelling wave predicted by the model. The transient in this case appears quite longer. The return maps, shown in figures 12(a,b) for $\varepsilon_1 = 0$, 0.003, 0.005 and 0.008, indicate again that the solution in linearly stable.

3.2   With transverse distributed load

In the presence of a transverse distributed constant load p the governing equations (41)-(42) possess a constant particular solution w_p given by

$$w_p = \frac{p}{k_1}, \quad \text{for} \quad p < 0, \tag{51}$$

$$w_p = \frac{p}{k_2}, \quad \text{for} \quad p > 0. \tag{52}$$
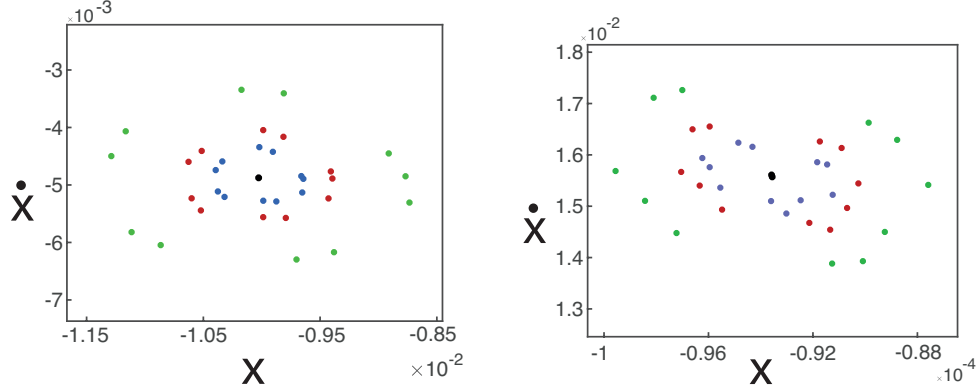
Figure 12: Return map with the initial condition (50) for $L = 1$, $a_0 = 0.01$, (a) $k_1 = 1, k_2 = 2$, (b) $k_1 = 1, k_2 = 5$ and $\varepsilon = 0$ (black dot), 0.003 (blue dots), 0.005 (red dots) and 0.008 (green dots).

It must be remarked that equation (40) possesses many particular solutions, most of which are incompatible with the propagating wave solutions we are dealing with.

To search for the numerical solution of equation (40) we subtract the particular solution given by (51) or (52) and approach numerically only the homogeneous equation with the associated initial - boundary value problem

$$\frac{\partial^2 u}{\partial t^2} - v^2 \frac{\partial^2 u}{\partial x^2} + \gamma(u + w_0)(u + w_p) = 0 \tag{53}$$

$$u(0, t) = \varphi(t) - w_p \tag{54}$$

$$u(x, 0) = w_0(x) - w_p; \qquad \frac{\partial u}{\partial t}(x, 0) = \psi(x) \tag{55}$$

where $u = w - w_p$. The values of α and a, which enter the numerical solution via the boundary condition $\varphi(t)$, are given by the solutions of the dispersion relation (47). As we have remarked in Section 2.3.3, equation (47) possesses a multiplicity of solutions for any given α. It turns out that only the lowest solution corresponds to a simple wave, while the higher ones correspond to multiple waves. The dispersion relation (47) is shown in Fig. 14(a-d) for $k_1 = 1, k_2 = 2$ and four different values of α; here $\alpha_{cr} = 0.585786$. The solutions, which give the value of a for a given α, form a countably infinite set and only the lowest one correspond to a simple wave. The first singularity corresponds to $a = \pi/\alpha_{cr}$; note how, by varying α, the position of the roots with respect to the singularities changes. In this work we are interested only in simple waves, that is in the lowest roots of the dispersion relation. The
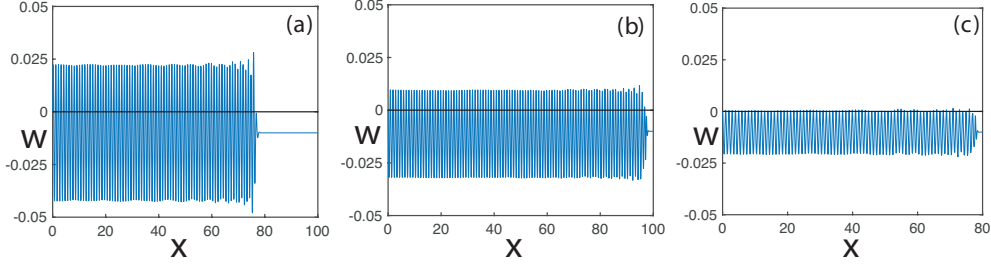
Figure 13: The solution $w(x,t)$ at the final time for (a) $k_1 = k_2 = 1$, (b) $k_1 = 1, k_2 = 2$, (c) $k_1 = 1, k_2 = 10$ and $L = 1, p = -0.01, \alpha = 1.2\,\alpha_{cr}$.
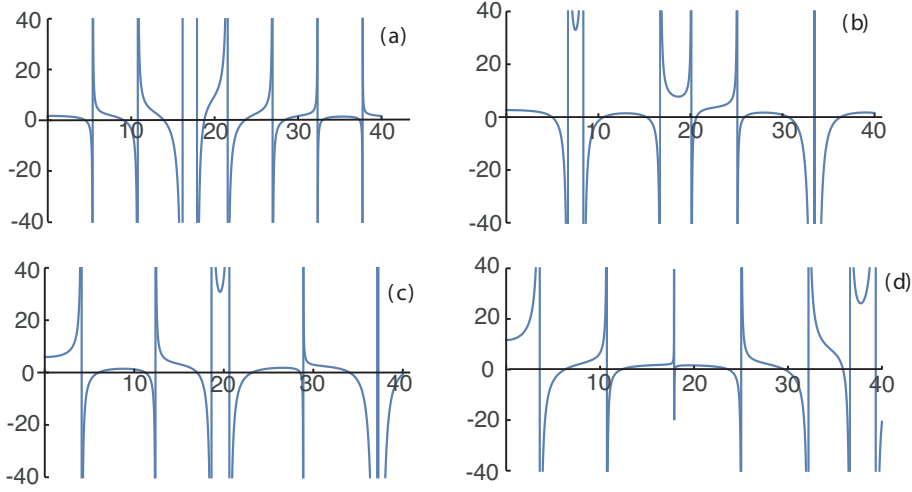

Figure 14: The dispersion relation (47) as function of a for $k_1 = 1, k_2 = 2$ and (a) $\alpha = 0.3\,\alpha_{cr}$, (b) $\alpha = 0.8\,\alpha_{cr}$, (c) $\alpha = 1.3\,\alpha_{cr}$ (d) $\alpha = 1.8\,\alpha_{cr}$.

presence of multiple roots, however, entails that the waves corresponding to the higher roots coexist with the fundamental one. As a consequence, the propagating traveling waves described by our model cannot be reproduced exactly by the numerical solution, because the numerical errors introduced by the discretization of the equations excite these higher waves. Because of this problem, the constant amplitude of the traveling wave presents a slight modulation.

The propagating wave solution $w(x,t)$ is portrayed in Figures 13(a-c) for $p = -0.01$, $L = 1$, $\alpha = 1.2\,\alpha_{cr}$ and (a) $k_1 = k_1 = 1$, (b) $k_1 = 1, k_2 = 2$, (c) $k_1 = 1, k_2 = 10$. In all three cases, we observe a similar behaviour as in the case without the transverse load: after an initial transient, the propagating wave settles to the right-propagating wave with constant amplitude, which
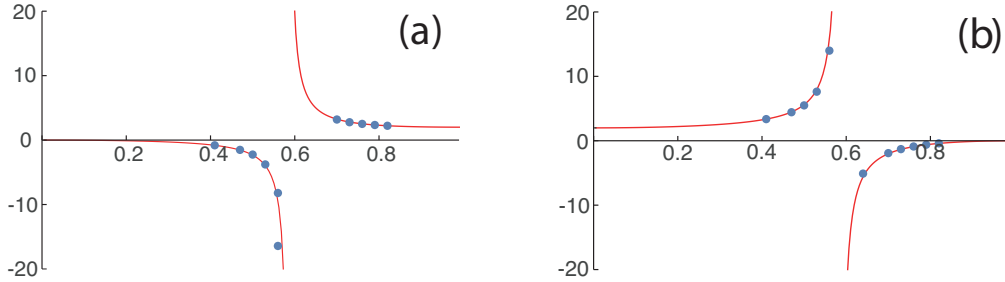
Figure 15: The maximum and miminum of $W(s)$ for $k_1 = 1, k_2 = 2$, varying $0 \leq \alpha \leq 1$. Here $\alpha_{cr} = 0.585786$.

is the restriction to $x \geq 0$ of the wave found analytically in Section 2.3.3.

In Fig. 15(a,b) we highlight the role of α_{cr} by showing the maximum excursions of W_1 and W_2, normalized to k_1/p and k_2/p respectively, as functions of α for $k_1 = 1$ and $k_2 = 2$, which results in $\alpha_{cr} = 0.585786$; the singularity in the amplitude at $\alpha = \alpha_{cr}$ and the requirement on the sign of the transversal load p are evident (see the discussion following equation (47)). In these figures, the red lines represent the theoretical result, obtained from equations (43) and (44) with the coefficients given by (45) with a and α related by the dispersion relation (47). The blue dots are the amplitudes calculated from the numerical solution; the agreement is excellent when α is far from α_{cr}, while for α close to α_{cr} the discretization errors become somewhat larger.
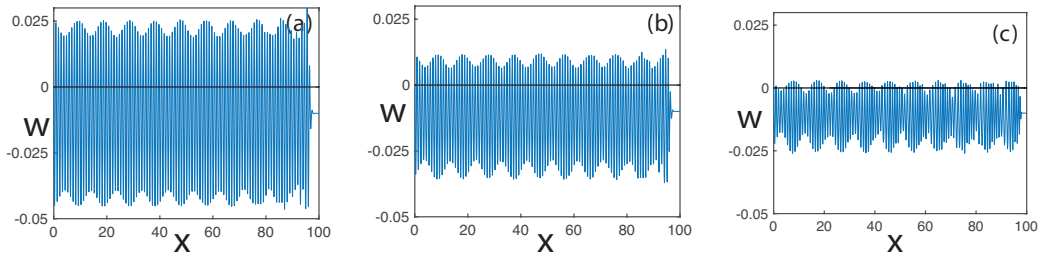

Figure 16: The solution $w(x,t)$ at the final time for (a) $k_1 = k_2 = 1$ (linear case), (b) $k_1 = 1, k_2 = 2$, (c) $k_1 = 1, k_2 = 10$ and $L = 1$, $p = -0.01$, $\alpha = 1.2\,\alpha_{cr}$, $\varepsilon = 0.003$ and $\omega_1 = 1.1\,\omega$.

Along the same lines followed in the homogeneous case, we study numerically the stability of the traveling wave solutions by introducing a small perturbation of the form (49) in the boundary condition. The solution is shown in figure 16(a-c) for (a) $k_1 = k_1 = 1$, (b) $k_1 = 1, k_2 = 2$ and (c) $k_1 = 1, k_2 = 10$,

23

$L = 1$, $p = -0.01$, $\alpha = 1.2\,\alpha_{cr}$. $\varepsilon = 0.003$ and $\omega_1 = 1.1\,\omega$. We observe the same behaviour seen in the case without load, namely an oscillating amplitude at a frequency corresponding to $\omega_1 - \omega$. The amplitude of the slower oscillations is proportional to ε. We obtain the same qualitative scenario for a wide range of parameters, k_1 and k_2, p, α and ω_1.
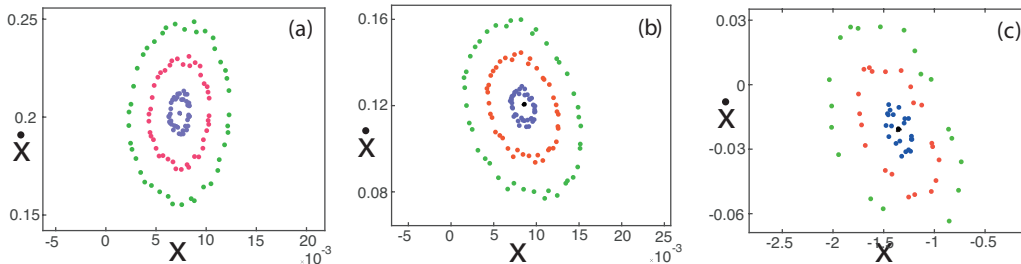

Figure 17: Return map (a) $k_1 = k_2 = 1$ (linear case), (b) $k_1 = 1, k_2 = 2$, (c) $k_1 = 1, k_2 = 5$, and $L = 1$, $p = -0.01$, $\alpha = 1.2\,\alpha_{cr}$, and $\omega_1 = \sqrt{2}\,\omega$ and $\varepsilon = 0$ (black dot), 0.001 (blue dots), 0.003 (red dots) and 0.005 (green dots).

Also in this case it is useful to show the return maps $(f(t), \dot{f}(t)) \to (f(t + \tau), \dot{f}(t + \tau))$. In figure 17 we have (a) $k_1 = k_2 = 1$, (b) $k_1 = 1, k_2 = 2$, (c) $k_1 = 1, k_2 = 5$ with $L = 1$, $p = -0.01$, $\alpha = 1.2\,\alpha_{cr}$, and $\omega_1 = \sqrt{2}\,\omega$ and $\varepsilon = 0$ (black dot), 0.001 (blue dots), 0.003 (red dots) and 0.005 (green dots). Again, the phase space points with $\varepsilon \neq 0$ lie on closed orbits around the unperturbed fixed point, indicating that the periodic traveling waves are stable also when a transversal distributed load is applied.

4   Conclusions

We have investigated theoretically and numerically the occurrence of periodic traveling waves supported by the wave equation with the addition of a nonlinear piecewise constant stiffness. In particular, we have studied periodic simple waves, which possess only one node internal to the periodicity interval. In the absence of an external distributed load, the propagation speed and the spatial extension of the two subintervals (a compression interval of size α, where the solution is negative and a tension interval of size $1 - \alpha$, where the solution is positive) are determined directly as functions of the values of the stiffnesses, while the amplitude of the waves in undetermined. When a distributed load is added, the size of the compression interval α becomes a free parameter, while the propagation speed is determined by the solution of a dispersion relation. The amplitude is then a function of α

24

and it exhibits a singularity when α equals the value of the case without load.

The properties of the solutions, without and with the external distributed load, have been verified by a direct numerical solution of the wave equation, obtained by a simple finite difference approach. The stability of these waves has also been studied by numerical means. We have introduced both time-histories and return maps; all our results indicate that the periodic travelling wave solutions are linearly stable, at least against the two kinds of perturbations considered here.

The nonlinearity introduced in the model by assumptions (13)-(14) when $k_1 \neq k_2$ produces the asymmetry of the wave profile with respect to the $w = 0$ baseline, as seen in the numerical simulations; it becomes more important in the limiting cases of unilateral and unilaterally rigid substrate. The nonlinearity causes also the deformation of the return-map orbits from the elliptical shape seen in the linear case ($k_1 = k_2$).

References

[1] S. Maezawa, Steady forced vibrations of unsymmetrical piecewise linear systems, Bulletin of the Japanese Society of Mechanical Engineering, 4:201-229, 1961.

[2] A.A. Andronov, A. Vitt, S.E. Khaikin, Theory of oscillators, Pergamon Press, Oxford, 1966. ISBN: 978-1-4831-6724-4

[3] M. Farshad, Stresses in rotating disks of materials with different compressive and tensile moduli, International Journal of Mechanical Sciences, 16(8):559-564, 1974.

[4] M. Di Bernardo, C. Budd, A.R. Champneys, P. Kowalczyk, Piecewise-smooth dynamical systems: theory and applications, Springer-Verlag, 2008. ISBN: 978-1-84628-708-4

[5] S. Shaw, P. Holmes. A periodically forced piecewise linear oscillator. Journal of Sound and Vibration, 90(1):129-155, 1983.

[6] J.M.T. Thompson, R. Ghaffari, Chaos after period doubling bifurcations in the resonance of an impact oscillator, Physics Letters 91(1):5-8, 1982.

[7] E. Freire, E. Ponce, F. Rodrigo, F. Torres, Bifurcation sets of continuous piecewise linear systems with two zones. Int. J. Bifurcation and Chaos, 8:2073–2097, 1998.

[8] H. Wolf, J. Kodvanj, S. Bjelovucić-Kopilović, Effect of smoothing piecewise linear oscillators on their stability predictions. Journal of Sound and Vibration, 270:917–932, 2004.

[9] V. Carmona, E. Freire, E. Ponce, F. Torres, The continuous matching of two stable linear systems can be unstable. Discrete and Continuous Dynamical Systems, 16:689–703, 2006

[10] S. Lenci, G. Rega, Periodic solutions and bifurcations in an impact inverted pendulum under impulsive excitation, Chaos, Solitons & Fractals, 11(15):2453-2472, 2000.

[11] S. Lenci, L. Demeio, M. Petrini, Response scenario and non-smooth features in the nonlinear dynamics of an impacting inverted pendulum, ASME J. Computation and Nonlinear Dynamics, 1(1): 56-64, 2005.

[12] S. Lenci, G. Rega, A dynamical systems approach to the overturning of rocking blocks," Chaos, Solitons & Fractals, 28(2):527-542, 2006.

[13] L. Pust, F. Peterka, Impact oscillator with Hertz's model of contact, Meccanica, 38:99-114, 2003.

[14] G. Stefani, M. De Angelis, U. Andreaus, Scenarios in the experimental response of a vibro-impact single-degree-of-freedom system and numerical simulations, Nonlinear Dynamics,) 103:3465–3488, 2021.

[15] S.-H. Shen, C. Pierre, Natural modes of Bernoulli-Euler beams with symmetric cracks, Journal of Sound and Vibration, 138:115-134, 1990.

[16] A. Morassi, Crack-induced changes in eigenparameters of beam structures, ASCE Journal of Engineering Mechanics, 119:1798-1803, 1993.

[17] M.N. Cerri, F. Vestroni, Detection of damage in beams subjected to diffused cracking, Journal of Sound and Vibration, 234(2):259-276, 2000.

[18] Y. Yan, Y. Liu, M. Liao, A comparative study of the vibroimpact capsule systems with one-sided and two-sided constraints. Nonlinear Dynamics, 89(2):1063-1087, 2017.

[19] S. Divenyi, M.A. Savi, M. Wiercigroch, E. Pavlovskaia, Drill-string vibration analysis using non-smooth dynamics approach. Nonlinear Dynamics, 70(2):1017-1035, 2012.

[20] S. Coombes, Neuronal networks with gap junctions: A study of piecewise linear planar neuron models. SIAM Applied Dynamical Systems, 7:1101–1129, 2008.

[21] L. Demeio, S. Lenci, Forced nonlinear oscillations of semi-infinite cables and beams resting on a unilateral elastic substrate, Nonlinear Dynamics, 49:203-215, 2007.

[22] N.C. Tsai, R.E. Westmann, Beams on tensionless foundation, ASCE Journal of Engineering Mechanics, 93:1-12, 1967.

[23] Z. Celep, A. Malaika, M. Abu Hussein, Forced vibrations of a beam on a tensionless elastic foundation, Journal of Sound and Vibration, 128:235-246, 1989.

[24] U. Bhattiprolu, A,k. Bajaj, P. Davies, Periodic response predictions of beams on nonlinear and viscoelastic unilateral foundations using incremental harmonic balance method, International Journal of Solids and Structures, 99:28–39, 2016.

[25] A.C. Scott, A nonlinear Klein-Gordon equation, American Journal of Physics, 37:52, 1969.

[26] H. Kolsky, Stress Waves in Solids, Dover, 1963. ISBN: 486-61098-5

[27] K.F. Graff, Wave Motion in Elastic Solids, Dover, 1975. ISBN: 0-486-66745-6

[28] M. Farshad, M. Shahinpoor, Beams on bilinear elastic foundations, International Journal of Mechanical Science, 14(7):441-445, 1972

[29] W. Johnson, V. Kouskoulas, Beam on bilinear foundation. Journal of Applied Mechanics, 40(1):239–243, 1973.

[30] M.A. Adin, D.Z. Yankelevsky, M. Eisemberger, Analysis of beams on a bi-moduli elastic foundation. Computer Methods in Applied Mechanics and Engineering, 49(3):319-330, 1985.

[31] Z.H. Liu, L. Wang, L.Z. Pan, Stability of beams on bi-moduli elastic foundation, Journal of Applied Mechanics, 68(4):668-670, 2001.

[32] P. Castro Jorge, A. Pinto da Costa, F.M.F. Simoes, Finite element dynamic analysis of finite beams on a bilinear foundation under a moving load, Journal of Sound and Vibration, 23:328-344, 2015.

[33] T. Mazilu, The dynamics of an infinite uniform Euler-Bernoulli beam on bilinear viscoelastic foundation under moving loads, Procedia Engineering, 199:2561-2566, 2017.

[34] D. Froio, Structural Dynamics Modelization of one-dimensional elements on elastic foundations under fast moving load, PhD Thesis, University of Bergamo, Italy, 2017.

[35] D. Froio, E. Rizzi, F.M.F. Simoes, A. Pinto Da Costa, Dynamics of a beam on a bilinear elastic foundation under harmonic moving load, Acta Mechanica, 229:4141-4165, 2018.

[36] Y. Zhang, X. Liu, Y. Wei, Response of an infinite beam on a bilinear elastic foundation: Bridging the gap between the Winkler and tensionless foundation models, European Journal of Mechanics / A Solids, 71:394-403, 2018.

[37] S. Lenci, Propagation of periodic waves in beams on a bilinear foundation, International Journal of Mechanical Sciences, 207:106656, 2021.

[38] D. Younesian, A. Hosseinkhani, H. Askari, E. Esmailzadeh, Elastic and viscoelastic foundations: a review on linear and nonlinear vibration modeling and applications, Nonlinear Dynamics, 97:853-895, 2019.

[39] A.V. Metrikine, Steady state response of an infinite string on a nonlinear visco-elastic foundation to moving point loads, Journal of Sound and Vibration, 272:1033-1046, 2004.

[40] O. Nicoletti, Symmetry breaking in metamaterials, Nature Materials, 13:843, 2014.

[41] K. Nagatou, M. Plum, P.J. McKenna, Orbital stability investigations for travelling waves in a nonlinearly supported beam, Journal of Differential Equations, 268:80-114, 2019.

[42] J. Shatah, Stable Standing Waves of Nonlinear Klein-Gordon Equations, Comm. Math. Phys., 91:313-327, 1983.

[43] P. Gravel and C. Gauthier, Classical applications of the Klein–Gordon equation, Am. J. Phys., 79:447, 2011.

[44] R. Chiappinelli, What Do You Mean by "Nonlinear Eigenvalue Problems"?, Axioms, 7:39, 2018.

[45] Betcke, T.; Higham, N.J.; Mehrmann, V.; Schroder, C.; Tisseur, F. NLEVP: A collection of nonlinear eigenvalue problems. ACM Trans. Math. Softw. 39:28, 2013.

[46] Berger, M.S. Nonlinearity and Functional Analysis; Academic Press: Cambridge, MA, USA, 1977.

[47] John, F. Partial Differential Equations; Springer Verlag: New York, NY, USA, 1986.